Optik - International Journal for Light and Electron Optics 288 (2023) 171160

Contents lists available at ScienceDirect

Optik

journal homepage: www.elsevier.com/locate/ijleo

Original research article

Investigation of the optoelectronic and structural properties of $FA_{(1-x)}Bi_xPbBr_6I_3$ of perovskite mixed halide films

Abdoulaye Touré [a,*], Amal Bouich [a,*], Youssouf Doumbia [a], Bernabe Mari Soucasse [a], Donafologo Soro [b]

[a] Institute of Design for Automated Manufacturing and Production, Polytechnic University of Valencia, Spain
[b] Department of Science and Technology-Ecole Normale Supérieure (ENS) of Abidjan Cote d'Ivoire, Ivory Coast, Spain

ARTICLE INFO

Keywords:
Perovskite
FAPbBr2I
Mixed
Band gap
Stability

ABSTRACT

In this study, we analyzed the structural and optical characteristics of pure *$FAPbBr_2I$* mixed halide perovskites and doped with a large proportion of bismuth. Previous work has demonstrated that the replacement of 2/3 of the iodine by bromine in the perovskite *$FAPbI_3$* limits its phase transition and thus increases its stability. However, this improvement in stability is accompanied by an increase in the band gap, from 1.45 to about 2 eV. It has been found that bismuth doping of certain perovskite materials makes it possible, in addition to increasing their stability, to significantly reduce their band gap, although certain authors still contest this phenomenon. Thus, we synthesized thin layers of perovskite *$FAPbBr_2I$* doped with bismuth and studied the effect of this doping on the crystalline structure and the layers' optical characteristics thanks to analyses by X-ray diffraction, scanning electron microscopy and measurements of absorption and photoluminescence. The structural analysis results showed that bismuth diffuses very slowly into the crystal, resulting in a reduction in crystal size and a smoother surface. Moreover, measurements of the absorption coefficient revealed a significant reduction in the band gap, going from 2.08 eV with 0% bismuth to 1.45 eV with 20% bismuth. However, photoluminescence measurements gave much higher bandgap values. We believe that a phenomenon related to the addition of bismuth is responsible for this discrepancy.

1. Introduction

The perovskite *$FAPbI_3$* is an exceedingly promising material for solar cells due to its high energy conversion efficiency and exceptional optical properties [1,2]. *$FAPbI_3$* refers to the formamidinium lead iodide, which is a type of hybrid organic-inorganic perovskite with a cubic crystalline structure. The material exhibits a narrow optical energy gap (~1.45 eV) and strong absorption of solar light, endowing it with high potential for solar energy conversion into electricity [3–5]. In 2021, a team of Korean researchers successfully fabricated a *$FAPbI_3$* -based solar cell with a high efficiency of up to 24.82% (certified at 24.64% with a voltage loss of 0.3 volts), and it appears to be a matter of time before surpassing the benchmarks set by inorganic semiconductors such as crystalline silicon and gallium arsenide [6–8]. They achieved these results by heating the perovskite layer after deposition for a short period at a high temperature to promote the formation of larger and more uniform crystals.

The long-term stability of *$FAPbI_3$* is a major issue for its practical application due to its rapid decomposition under environmental

* Corresponding authors.
E-mail addresses: tabdoul@doctor.upv.es (A. Touré), ambo1@doctor.upv.es (A. Bouich).

https://doi.org/10.1016/j.ijleo.2023.171160
Received 13 April 2023; Received in revised form 23 May 2023; Accepted 9 July 2023
Available online 10 July 2023
0030-4026/© 2023 The Authors. Published by Elsevier GmbH. This is an open access article under the CC BY-NC-ND license (http://creativecommons.org/licenses/by-nc-nd/4.0/).

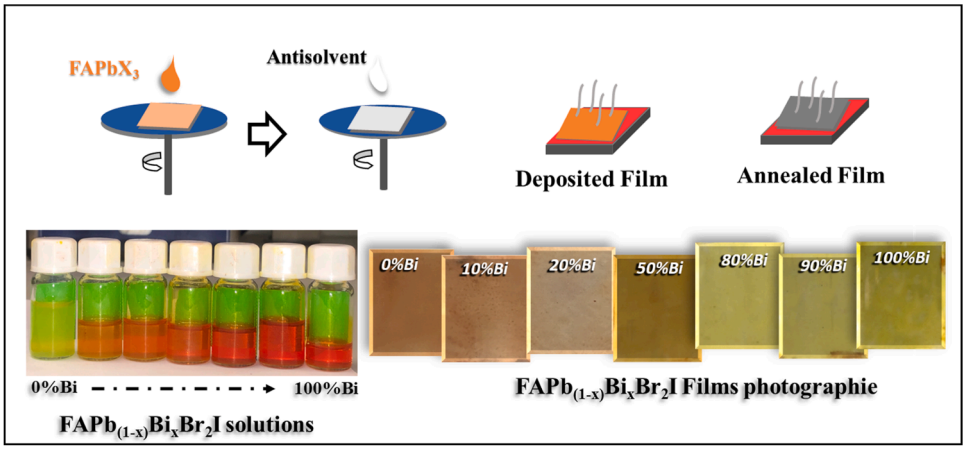

Fig. 1. : Synthesis method of $FAPb_{(1-x)}Bi_xBr_2I$ films where $x = \{0, 0.1, 0.2, 0.5, 0.8, 0.9, and\ 1\}$.

conditions, stemming from its sensitivity to moisture and tendency to phase change at ambient temperature [9–11]. $FAPbI_3$ stabilizes in the form of non-perovskite yellow active phase (δ- $FAPbI_3$) in a hexagonal crystalline system at low temperature, and the required cubic perovskite black phase (α- $FAPbI_3$) can only be obtained and maintained at high temperature ($150^{\circ}C$) [12–19]. Over the years, several approaches have been proposed to improve the stability of $FAPbI_3$, including modification of the interface structure, modification of the transport layer composition [20,21], optimization of the preparation method [22–27], addition of stabilizing cations [28], and partial or total halogen substitution [29–31].

Partial halogen substitution involves replacing a portion of the halogen in the perovskite composition with another halogen of different size [32]. This substitution can improve the thermal stability and moisture stability of the perovskite [33]. In one of our previous studies [34], we showed that mixing the halogen iodine (I^-) with bromine (Br^-) or chlorine (Cl^-) can improve the stability of $FAPbX_3$ to humidity and limited the phase transition. In [34] we showed that the $FAPbBr_2I$ mixed perovskite was the best compromise in terms of stability and optical properties. This mixed perovskite absorbs visible light well even after a fairly long time of exposure to ambient temperature and humidity conditions. But the FAPbBr2I has a too wide band gap of about 1.8 eV far from the ideal value for photovoltaic applications of 1.45 eV. In this manuscript we aim to reduce the band gap of $FAPbBr_2I$ while preserving its structural properties through doping by Bismuth.

Doping is a widely used method to improve the properties of semiconductor materials, including perovskites [35–38]. In the case of $FAPbI_3$, doping with elements such as bismuth (Bi) has been studied to improve the stability and performance properties of the material.

Studies have shown that incorporating bismuth into the perovskite structure compounds can improve them thermal stability and lifetime by regenerating defect sites and limiting decay to volatile halogens. Moreover, bismuth doping can also increase the electrical conductivity and reduce the bandgap, thereby improving the energy conversion efficiency of perovskite solar cells [39–41]. However, the effect of doping depends on the concentration of bismuth and the doping method used. High concentrations can cause degradation in crystal quality and overall solar cell performance [42].

In this study, we observed the effect of bismuth on the optoelectronic and structural properties of the mixed halide perovskite $FAPbBr_2I$. To achieve this goal, we synthesized thin films of the perovskite by varying the bismuth percentages from 0% to 100%. We used several characterization techniques, such as X-ray diffraction (XRD), scanning electron microscopy (SEM), absorbance measurement, and photoluminescence measurement, to analyze and interpret the optical and structural properties of the produced thin films. By measuring the evolution of the band gap as a function of bismuth concentration in the perovskite materials, we hope to determine how far the band gap can be modified by this method and establish the mechanisms responsible for this reduction. The aim is to design an optimized material that combines all the necessary properties for industrial production of perovskite-based panels.

2. Materials and methods

2.1. Materials

The $FAPbBr_2I$ samples were prepared using commercial precursors purchased from a supplier (Sigma-Aldrich). The precursors used were formamidinium iodide (FAI), formamidinium bromide ($FABr$), lead iodide (PbI_2), lead bromide ($PbBr_2$) and bismuth bromide ($BiBr$) of 99.9% purity each. Solvents such as dimethyl sulfoxide (DMSO) and dimethylformamide (DMF) were used as well as diethyl ether as an anti-solvent. We used silicon oxide (SiO_2) glass substrates coated with fluorine-doped tin oxide (FTO).

2.2. Film preparation

To obtain better quality films, the substrate must be properly treated. To this end, we cleaned the substrates using the following

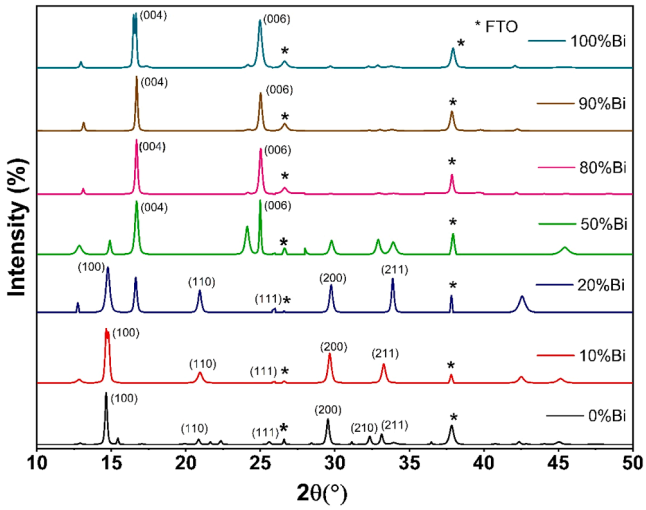

Fig. 2. : *XRD* measurements of $FAPb_{(1-x)}Bi_xBr_2I$ layers where $x = \{0, 0.1, 0.2, 0.5, 0.8, 0.9 \text{ and } 1\}$.

method:

First, we immersed the fluorine-doped tin oxide (FTO) coated glass substrates in an aqueous solution of 100 *mL* of ellmanex III (2 *mL* of ellmanex and 98 *mL* of distilled water) and subjected them to ultrasound for 15 min. They were then immersed in ethanol and subjected to ultrasound for an additional 15 min. After ethanol, we used acetone, still subjected to ultrasound.

Finally, the last solution used was isopropanol, also subjected to ultrasound for 15 min each time. After the solution steps, we used pressurized air to dry the substrates before placing them in the OSILA apparatus for an additional 15 min. For the preparation of the perovskite solution, we dissolved methylamonium bromide (*FABr*), lead dibromide ($PbBr_2$) in the solvent dimethylformamide (DMF) and bismuth bromide (*BiBr*) from 0%, 10%, 20%, 50%, 80%, 90% and 100% by weight of *FABr* and formamidinium iodide (*FAI*) in the solvent dimethylsulfoxide (DMSO). The different $FA_{(1-x)}BixPbBr_6I_3$ solutions are then deposited on the rotating substrate by the one-step spin-coating method. The substrates are rotated at 5000 rpm for 30 s. Ether was used as an anti-solvent. The samples were annealed at 80°*C* for 20 min on a hot plate. The amount of precursors used was calculated using Eq. 1.

$$(2x+1)FAI + (1-x)PbBr_2 + 2xBiBr_3 \rightarrow \quad (1-x)FAPbBr_2I + xFA_3Bi_2Br_6I_3 \tag{1}$$

With $x = \{0;0.1;0.2;0.5;0.8;0.9;1\}$ the Bismuth portion. Fig. 1.

2.3. Characterization techniques

The analysis of the samples involves the use of several characterization techniques:

- X-ray diffraction (XRD) analysis was performed using the RIGAKU-Ultima IV diffractometer. The CuKα beam with a wavelength of 1.54 Å was used as the X-ray source. 2Θ angle scans between 10° and 60° were performed.
- Using the scanning electron microscope (SEM), surface images of the different thin films were made.
- UV–visible absorption measurements were carried out using the HR2000 spectrophotometer. For all measurements, a spectrum from 300 *nm* to 900 *nm* was applied.

3. Results and discussions

3.1. Structural analysis

The X-ray diffraction pattern of the synthesized perovskite is shown in Fig. 2. FAPbBr2I appears to be effectively crystallized in a cubic system as also found in the literature [34]. According to Fig. 2, the XRD of all the thin films produced shows two main peaks corresponding to the preferred crystallographic orientations of the thin films. For the 0%, 10%, and 20% layers these peaks are located at 2θ angles of 14.5° and 29.4° for the (*100*) and (*200*) crystallographic planes respectively. It should be noted that the (*200*) plane is a repetition of the (*100*) plane so it is the same crystallographic orientation. The 20% *Bi* layer has a third main peak linked to the (*211*) plane and is located almost at 34°. In addition to the two main peaks, these thin films have other small peaks located at 21°, 25.8°, and 34° corresponding to the (*110*), (*111*), and (*211*) planes. As for the 50%, 80%, 90%, and 100% thin films, we have only two peaks of almost the same size which can be located at 16.5° and 25.3° characteristic of the Muller indices (*004*) and (*006*). This shows that the latter has two preferred crystallographic orientations. The Debye-Scherrer equation (Eq. 2) was used to calculate the crystal diameters for the seven samples from the X-ray diffraction peaks by measuring the maximum widths at half-maximum (FWHM) of the (*100*) and

Table 1
Grain diameters, dislocation density, and lattice strain of perovskite $FA_3Pb_{(1-x)}Bi_xBr_2I$ thin films where x = *{0, 0.1, 0.2, 0.5, 0.8, 0.9 and 1}*.

Samples	*D (nm)*	δ ($10^{-4}nm^{-2}$)	ε (10^{-3}_{rad})
$FAPbBr_2I$-Pure	97.89	1.04	1.61
$FAPbBr_2I$-10%Bi	74.28	1.81	2.57
$FAPbBr_2I$-20%Bi	83.85	1.42	2.37
$FAPbBr_2I$-50%Bi	78.35	1.63	2.90
$FAPbBr_2I$-80%Bi	87.48	1.31	2.03
$FAPbBr_2I$-90%Bi	95.99	1.09	2.38
$FA_3Bi_2Br_6I_3$.Pure	107.50	0.86	2.18

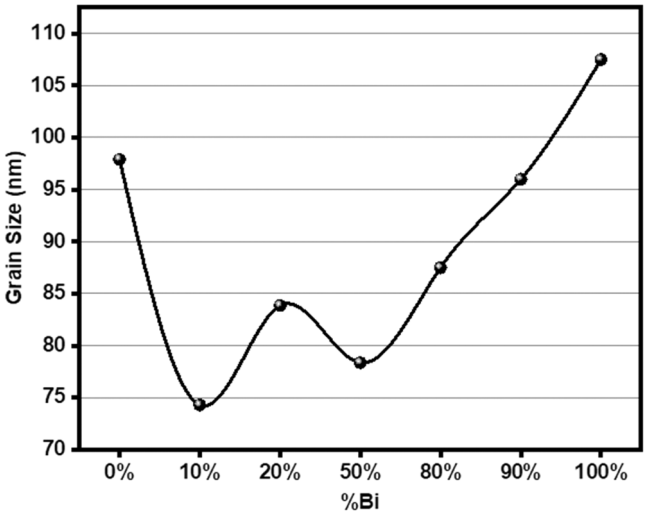

Fig. 3. : Crystallite size of $FA_3Pb_{(1-x)}Bi_xBr_2I$ films where $x = \{0, 0.1, 0.2, 0.5, 0.8, 0.9 \text{ and } 1\}$.

(*200*) planes for the pure and 10% and 20% doped samples and the (*004*) and (*006*) planes for all other doped samples.

$$D = \frac{K\lambda}{\beta \text{coscos} \quad \theta} \tag{2}$$

$\lambda = 0.15406\ nm$: the wavelength of the ray, β is the FWHM; θ: Bragg angle and K= 0.9.

The grain defects and strains in the thin film (Eq. 3) and the dislocation density (Eq. 4) of the crystal lattice were calculated. The values obtained are presented in Table 1.

$$\varepsilon = \frac{\beta}{4 \text{ tantan} \quad \theta} \tag{3}$$

$$\delta = \frac{1}{D^2} \tag{4}$$

The average crystal sizes, calculated by the Debye-Scherrer equation, are shown in Fig. 3. The larger the crystal size, the better the thin film. This is because the roughness increases with the grain size, which favors the trapping of light and thus the creation of electron-hole pairs. The unmixed samples have the largest crystals.

The unmixed samples have the largest crystals. The larger the crystal size, the better the thin film. Indeed, the roughness increases with the size of the grains, which favors the trapping of light and therefore the creation of electron-hole pairs. The crystals in the unmixed *$FAPbBr_2I$* thin film have an average diameter of about 98 *nm* compared to 107.5 *nm* for the *$FA_3Bi_2Br_6I_3$*-Pure film. The addition of up to 20% Bismuth to *$FAPbBr_2I$* reduces the crystal size considerably. With only 10% bismuth, the crystal size decreases by about 25%. Bismuth has a higher electron affinity than lead, which can change the distribution of electrons in the material and affect grain growth. A slight increase in grain size is observed with 20% bi, from 74 *nm* to 84 *nm*. This increase may be due to the presence, in almost the same proportions, of the two phases observed by X-ray diffraction. Beyond that, the grain size increases with the amount of bismuth, from 84 *nm* at 20% bismuth to 107.5 *nm* for *$FA_3Bi_2Br_6I_3$*-Pure.

The growth of crystals is influenced in particular by various factors such as solvent evaporation and thermodynamic driving forces. The incorporation of bismuth can alter the thermodynamic stability of the material. Studies have shown that the addition of certain dopants can reduce the phase transition temperature, which can influence the size of crystals formed during synthesis [1,2].

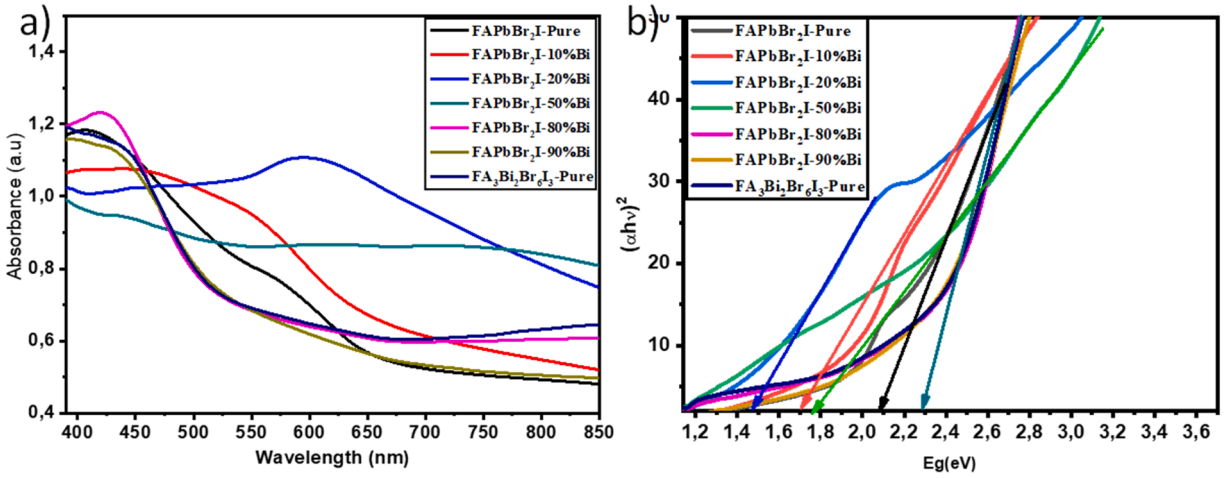

Fig. 4. : a) Absorbance spectra for perovskite $FA_3Pb_{(1-x)}Bi_xBr_2I$ films where $x = \{0, 0.1, 0.2, 0.5, 0.8, 0.9 \text{ and } 1\}$ b) band gap calculated for perovskite $FA_3Pb_{(1-x)}Bi_xBr_2I$ films where $x = \{0, 0.1, 0.2, 0.5, 0.8, 0.9 \text{ and } 1\}$.

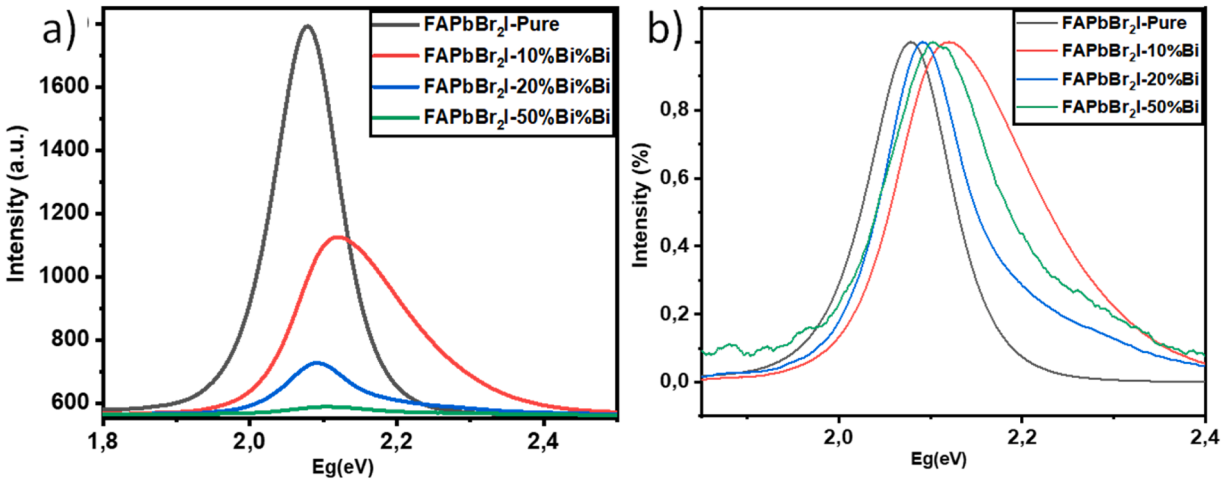

Fig. 5. : a) Photoluminescence (PL) for perovskite $FA_3Pb_{(1-x)}Bi_xBr_2I$ films where $x = \{0, 0.1, 0.2, 0.5, 0.8, 0.9 \text{ and } 1\}$ b) Normalized PL for perovskite $FA_3Pb_{(1-x)}Bi_xBr_2I$ films where $x = \{0, 0.1, 0.2, 0.5, 0.8, 0.9 \text{ and } 1\}$.

Also, bismuth may have limited solubility in the solvents used. When the concentration of bismuth exceeds a certain threshold, it can become less soluble, resulting in precipitation of additional bismuth particles. This precipitation can disrupt the growth of crystals and lead to a decrease in their size. Experimental studies on crystal temperature and solvents could greatly improve crystal size.

3.2. Absorbance and photoluminescence analysis

The analysis of the visible light absorption of the processed thin film samples is very important as they are manufactured as the absorbing layer of the solar cell. We analyzed the UV–visible light absorption of all samples with wavelengths between 300 *nm* and 900 *nm*. Fig. 4, shows that the absorbance of the samples varies very little between the wavelengths of 400 and 500 *nm*. Above 500 *nm*, the 20% *Bi* sample peaks at 1.2 at 620 nm and gradually decreases to 0.7 at 850 *nm*. Although it is important to study the absorption of thin films, it is even more necessary to study their ability to generate excitons (electron-hole pairs). With this in mind, we have been interested in the band gaps of the various thin films we have fabricated. The band gaps are plotted using the Tauc method. The band gaps vary between 1.44 *eV* and 2.3 *eV*. The smallest band gap is that of the 20% *Bi* thin film while the largest band gap is that of the 90% and 100% *Bi* thin films. This allows us to say that the 20% *Bi* thin film is the one that creates electron-hole pairs more easily and that the 90% and 100% *Bi* thin films create excitons a little more difficult compared to the other layers. The unmixed samples, *FAPbBr*$_2$*I*-pure and $FA_3Bi_2Br_6I_3$-pure show band gaps of 2.08 and 2.3 *eV* respectively. A reduction in the band gap value is observed, which decreases more or less linearly with increasing bismuth concentration up to 20%. Above 20%, the band gap increases, stabilizing at 2.3 *eV* from 80% bismuth.

Table 2
Optical properties of $FA_3Pb_{(1-x)}Bi_xBr_2I$ thin films where $x = \{0, 0.1, 0.2, 0.5, 0.8, 0.9 \text{ and } 1\}$.

Samples	Optical Band Gap by Absorption		Emission PL Peak		Anti-Stokes Shift
	λ (nm)	Eg (eV)	λ (nm)	Eg (eV)	(meV)
$FAPbBr_2I$-Pure	596	2.08	539	2.30	**219.06**
$FAPbBr_2I$-10%Bi	752	1.65	530	2.34	**690.95**
$FAPbBr_2I$-20%Bi	855	1.45	536	2.31	**862.48**
$FAPbBr_2I$-50%Bi	697	1.78	534	2.32	**543.79**
$FAPbBr_2I$-80%Bi	537	2.31	-	-	-
$FAPbBr_2I$-90%Bi	537	2.31	-	-	-
$FA_3Bi_2Br_6I_3$-Pure	539	2.3	-	-	-

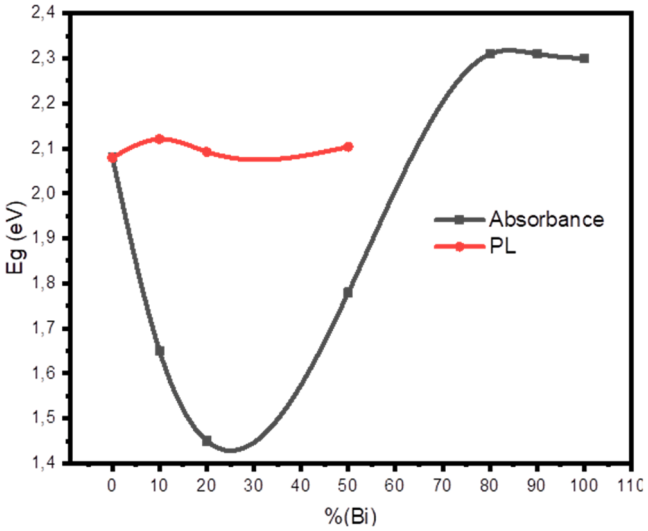

Fig. 6. : Bandgap values for different amounts of bismuth in $FA_3Pb_{(1-x)}Bi_xBr_2I$ layers measured by absorption and photoluminescence.

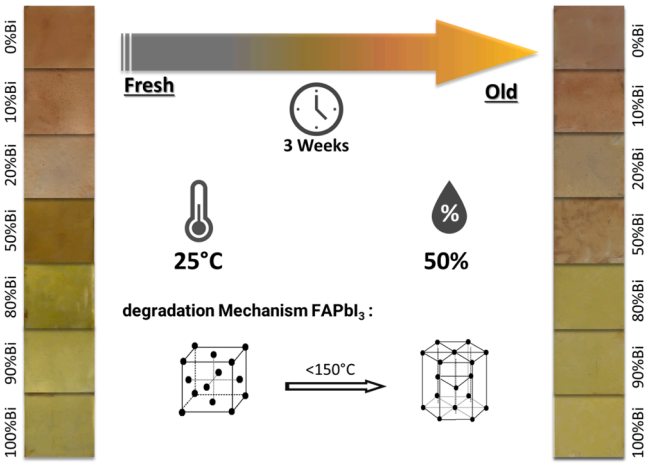

Fig. 7. : The degradation mechanism and pictures of fresh and aged films.

But after measuring the photoluminescence of our samples (Fig. 5), we found that the wavelength of the emitted photons does not match the energies estimated from the absorbance measurement. The PL measurements of samples containing 0%, 10%, 20%, and 50% *Bi* show a very slight fluctuation of the band gap. A small red shift is observed for the sample with 10% *Bi*. Table 2 and Fig. 6 show the measured band gap values from absorption and photoluminescence measurements. This phenomenon was also observed by the authors in [43–51].

This could be due to an indirect band gap [52,53] In materials with an indirect bandgap, the creation or annihilation of an electron

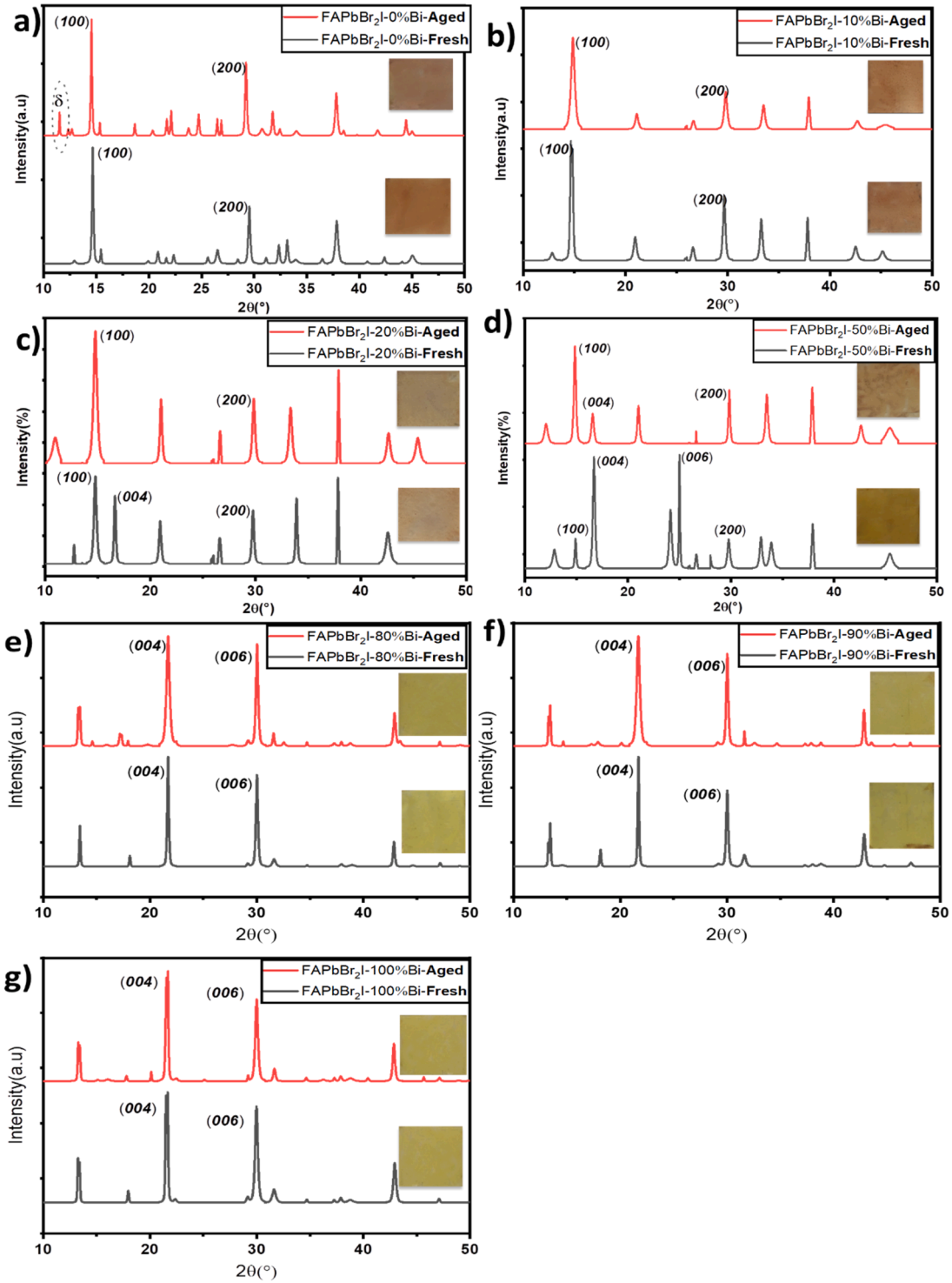

Fig. 8. : Comparative XRD plots of fresh and 3-week-old $FA_3Pb_{(1-x)}Bi_xBr_2I$ thin films where $x = \{0, 0.1, 0.2, 0.5, 0.8, 0.9 \text{ and } 1\}$.

hole cannot be obtained directly by absorption or emission of photons. Instead, electrons and holes must be created or annihilated by a series of phonon transitions. These phonon transitions involve the absorption or emission of photons of wavelength shorter than the bandgap, which can lead to a shift between the wavelength of the emitted photons and the bandgap. Also, the emitted photons have more energy than the absorbed photons, this anti-Stokes shift is the extra energy that can come from the dissipation of thermal phonons in the crystal lattice, cooling the crystal in the process.

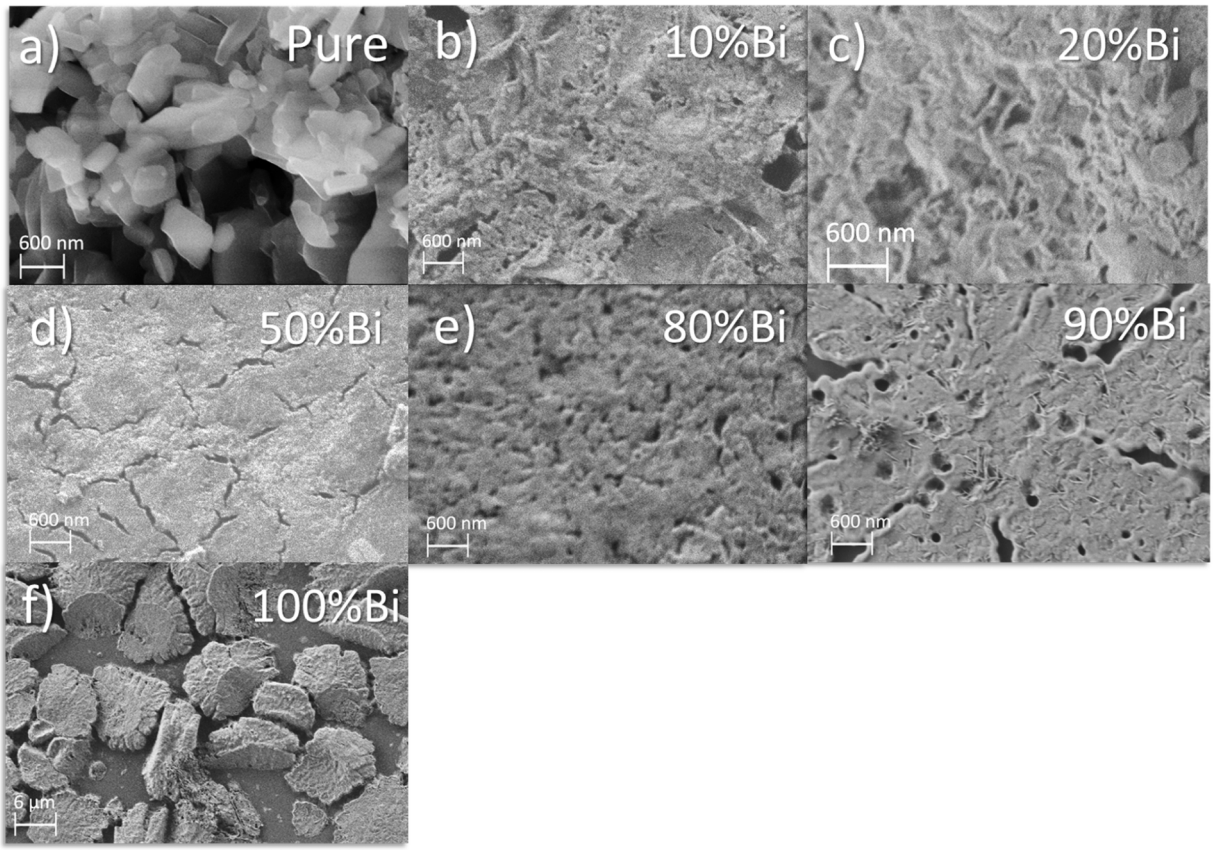

Fig. 9. : *FESEM* images of Aged $FA_3Pb_{(1-x)}Bi_xBr_2I$ thin films where $x = \{0, 0.1, 0.2, 0.5, 0.8, 0.9 \text{ and } 1\}$.

Lozhkina and these cooperators discuss this difference in [54]. They discuss the concept of band gap engineering for heterovalent doping of Bi^{3+} in $CsPbBr_3$ halide perovskites. The authors used molecular dynamics simulations to study the effects of doping on the electronic and structural properties of $CsPbBr_3$. They concluded that heterovalent doping of Bi^{3+} does not alter the band gap of $CsPbBr_3$. The Tauc method used for determining the band gap of the samples is based on arbitrary assumptions, making the method invalid for studying bismuth-doped perovskites.

This difference may also be caused by the presence of *Bi* dopant-induced deep trap states, with Bi^{3+} acting as an electron trap. This is the conclusion of the authors in [55], A study on trapping and conduction of charge carriers in chemically doped $MAPbBr_3$ perovskite films with bismuth. The addition of bismuth has no effect on the bandgap or exciton binding energy of the host $MAPbBr_3$ perovskite. However, Bi acts as a donor and pushes the Fermi level closer to the conduction band. This change promotes the formation of halogen interstitials, which are the true recombination centers. This can be perceived by absorption measurement as a change of the band gap.

Beyond 20% bismuth, the band gap increases very quickly from 1.78 eV to 50% Bi to 2.3 eV to 90% Bi. An overabundance of bismuth could lead to the formation of larger defects, thus increasing the band gap. At too high concentrations of bismuth (>20%), it is possible that the dopant no longer diffuses into the material. Bismuth aggregates form, creating local variations in the composition and structure of the material. Bismuth atoms interact with each other, forming complexes or structures specific to bismuth. Beyond 20% Bismuth, the optical properties of the layer tend more towards the optical characteristics of a pure bismuth layer.

4. Degradation study

Perovskite degradation under environmental conditions is a major obstacle to the commercialization or even industrialization of solar cells using this substance as an absorber layer. In the event that this instability is highlighted by a photographic analysis of $FAPbBr_2I$ layers exposed for three weeks at 50% humidity in a dark environment, Fig. 7. The results show that the undoped and doped $FAPbBr_2I$ layers do not undergo any significant color change. However, the layer doped with more than 50% Bismuth shows a change in its initial color from a yellow color due to the presence of higher percentage of Bismuth to a reddish color similar due to degradation of the perovskite structure.

XRD measurements carried out on perovskite samples exposed to ambient conditions for 3 weeks showed detailed results that varied according to the samples analyzed, Fig. 8. For the undoped sample, peaks related to the (*100*) and (*200*) crystallographic planes of the cubic phase remained present and intense, but the appearance of new low-intensity peaks related to a hexagonal phase was

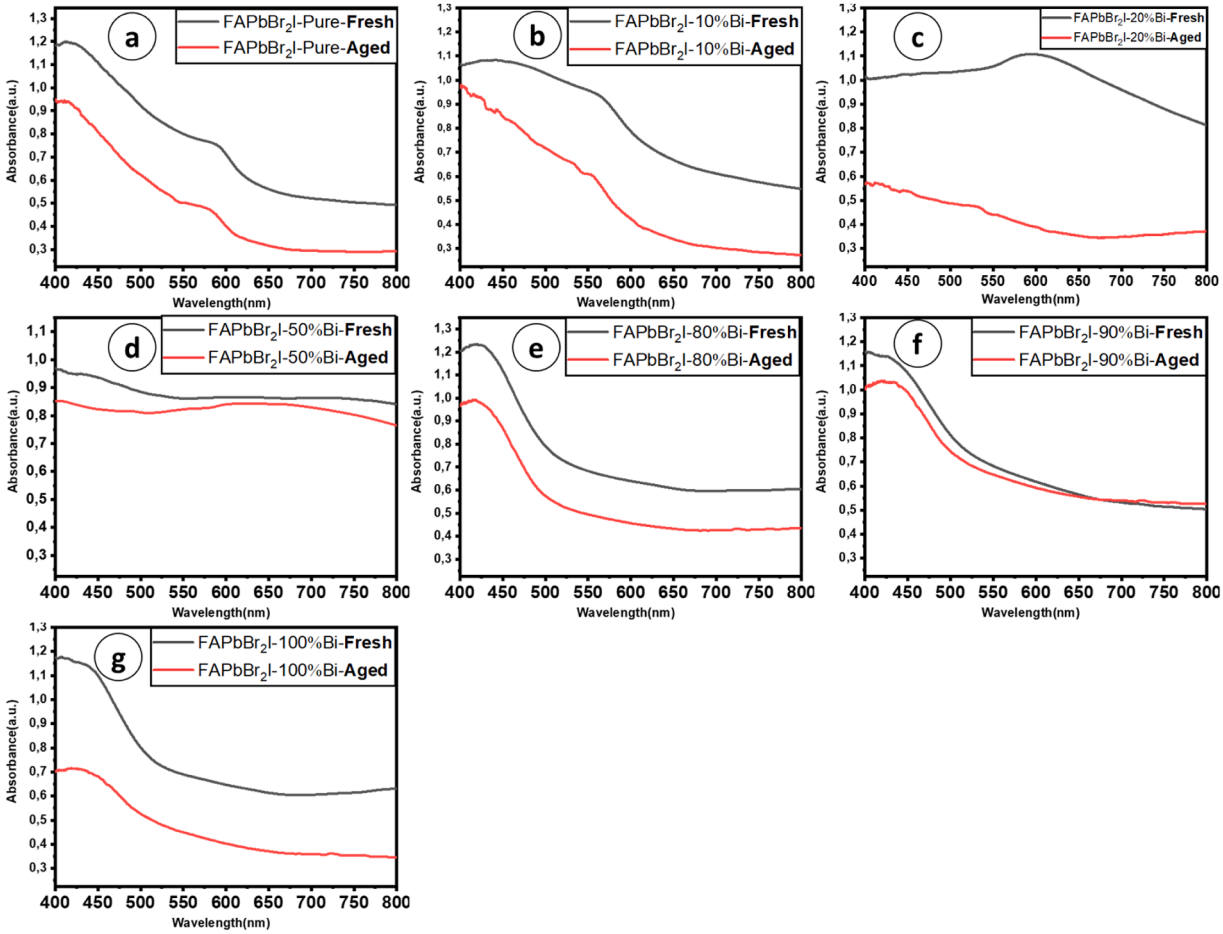

Fig. 10. : *The absorption spectra of fresh and aged perovskite samples $FA_3Pb_{(1-x)}Bi_xBr_2I$ thin films where x = {0, 0.1, 0.2, 0.5, 0.8, 0.9 and 1}.*

observed, indicating a small change in the crystal structure over time. For the sample containing 10% bismuth, the (*100*) and (*200*) peaks of the cubic phase remained present and intense and there was no appearance of new phases, but a decrease in the intensity of the diffraction peaks was observed. For the third sample, a stabilization of the crystal structure was observed favoring the cubic phase, with an increase in the intensity of the peaks corresponding to the (*100*) and (*200*) planes and a decrease in the peaks related to the hexagonal phase, which can be explained by the phenomenon of bismuth diffusion in the perovskite layer. The layer doped with 50% *Bi* shows the same phenomenon as with 20% *Bi*. An increase in the characteristic peaks at the (*100*) and (*200*) planes and a decrease in the characteristic peaks at the (*004*) and (*006*) planes are observed. *$FAPbBr_2I$*, even without dopant, shows better stability than *$FAPbI_3$* which degrades very quickly at low temperatures. Moreover, the diffractograms show that bismuth diffuses very slowly into the perovskite layer. This diffusion continues even after 3 weeks of exposure to the open air for the 20% and 50% doped samples.

The analysis of the surface morphology is important in that it tells us more or less about the reflectivity of thin films. The rougher the surface of the layers, the better the layer, i.e. rougher surfaces reflect less light and allow light to be trapped, which is the desired effect.

The surface morphology of *$FAPbBr_2I$* perovskites was studied using SEM (Fig. 9). Like the XRD analysis, As previously predicted with the Debye-Scherrer equation, the presence of synthesized nanoparticles is confirmed by the pictures. The morphology varies enormously with the amount of bismuth (Table 1, Eq. 2, and Fig. 3). The pure samples (*$FAPbBr_2I$*-pure and *$FA_3Bi_2Br_6I_3$*) show relatively rough surfaces, 100% Bismuth with the largest crystals. All the other samples obtained by mixing lead and bismuth have fairly smooth surfaces except for the 20% bismuth sample which remains very slightly rough. Fig. 10.

The different comparisons of absorption coefficients of fresh and aged samples are shown in Fig. All the samples show, except the sample with 20% bismuth, a decrease in absorption with a difference which decreases with the increase in the proportion of bismuth. The sample with 20% bismuth is the only one to show a significant decrease in absorption. Indeed, after 3 weeks of exposure, the samples had less dark color than at the start. This change is more marked for the sample with 20% bismuth [56–58].

5. Conclusion

Thin layers of Bismuth-doped $FAPbBr_2I$ perovskite were synthesized with the spin-coaching technique. The effect of bismuth on the optical characteristics and the crystalline structure of the layers were studied by XRD analysis, SEM, measurement of absorption, and photoluminescence. This analysis showed that the addition of bismuth causes a reduction in particle size due to the very slow diffusion of bismuth and effectively reduces the band gap. The analysis of the UV–visible absorption measurement data by Tauc's method, effectively shows that the band gap of $FAPbBr_2I$ decreases significantly with the increase in the concentration of bismuth, with a reduction of 0.63 eV between the concentration of 0% and 20% Bismuth. But the emitted photons, measured by photoluminescence, have more energy than the absorbed photons, this anti-Stokes shift; is the extra energy that possibly comes from the dissipation of thermal phonons in the crystal lattice, which could cool the crystal in the process.

Declaration of Competing Interest

The authors declare that they have no known competing financial interests or personal relationships that could have appeared to influence the work reported in this paper.

Data availability

The authors do not have permission to share data.

Acknowledgments

The author Amal Bouich acknowledges MCIN for funding support through Margarita Salas Fellowship (MCIN/AEI/10.13039/501100011033). This research has been funded by Grant PID2019-107137RB-C22 funded by MCIN/AEI/10.13039/501100011033 and by `` ERDF A Way of Making Europe.

References

[1] Y. Vaynzof, The future of perovskite photovoltaics—thermal evaporation or solution processing? Adv. Energy Mater. 10 (48) (2020), 2003073.
[2] J.V. Milić, S.M. Zakeeruddin, M. Grätzel, Layered hybrid formamidinium lead iodide perovskites: challenges and opportunities, Acc. Chem. Res. 54 (12) (2021) 2729–2740.
[3] K.P. Goetz, A.D. Taylor, F. Paulus, Y. Vaynzof, Shining light on the photoluminescence properties of metal halide perovskites, Adv. Funct. Mater. 30 (23) (2020), 1910004.
[4] Jongchul Lim, et al., Elucidating the long-range charge carrier mobility in metal halide perovskite thin films, Energy Environ. Sci. 12 (1) (2019) 169–176.
[5] C. Wehrenfennig, G.E. Eperon, M.B. Johnston, H.J. Snaith, L.M. Herz, High charge carrier mobilities and lifetimes in organolead trihalide perovskites, Adv. Mater. 26 (10) (2014) 1584–1589.
[6] Jeong, M. , Choi, I.W. , Go, E.M. , Cho, Y. , Kim, M. , Lee, B. , Yang , C. (2020). Stable perovskite solar cells with efficiency exceeding 24.8% and 0.3-V voltage loss. Science, 369(6511), 1615–1620.
[7] Osbel Almora, et al., Device performance of emerging photovoltaic materials (Version 3), Adv. Energy Mater. 13 (1) (2023), 2203313.
[8] Pabitra K. Nayak, et al., Photovoltaic solar cell technologies: analysing the state of the art, Nat. Rev. Mater. 4 (4) (2019) 269–285.
[9] S. Jiang, Y. Luan, J.I. Jang, T. Baikie, X. Huang, R. Li, J. Fang, Phase transitions of formamidinium lead iodide perovskite under pressure, J. Am. Chem. Soc. 140 (42) (2018) 13952–13957.
[10] M. Wang, F. Cao, L. Meng, M. Wang, L. Li, Phase-transition-cycle-induced recrystallization of FAPbI3 film in an open environment toward excellent photodetectors with high reproducibility, Adv. Sci. 9 (34) (2022), 2204386.
[11] A. Bouich, S. Ullah, B. Marí, L. Atourki, M.E. Touhami, One-step synthesis of FA1-xGAxPbI3 perovskites thin film with enhanced stability of alpha (α) phase, Mater. Chem. Phys. 258 (2021), 123973.
[12] W.C. Qiao, J.Q. Liang, W. Dong, K. Ma, X.L. Wang, Y.F. Yao, Formamidinium lead triiodide perovskites with improved structural stabilities and photovoltaic properties obtained by ultratrace dimethylamine substitution, NPG Asia Mater. 14 (1) (2022) 49.
[13] H. Chen, Y. Chen, T. Zhang, X. Liu, X. Wang, Y. Zhao, Advances to high-performance black-phase FAPbI3 perovskite for efficient and stable photovoltaics, Small Struct. 2 (5) (2021), 2000130.
[14] Y. Huang, X. Lei, T. He, Y. Jiang, M. Yuan, Recent progress on formamidinium-dominated perovskite photovoltaics, Adv. Energy Mater. 12 (4) (2022), 2100690.
[15] Y. Chen, N. Wei, Y. Miao, H. Chen, M. Ren, X. Liu, Y. Zhao, Inorganic CsPbBr3 perovskite nanocrystals as interfacial ion reservoirs to stabilize FAPbI3 perovskite for efficient photovoltaics, Adv. Energy Mater. 12 (16) (2022), 2200203.
[16] M. Lai, T. Lei, Y. Zhang, J. Jin, J.A. Steele, P. Yang, Phase transition dynamics in one-dimensional halide perovskite crystals, Mrs Bull. 46 (4) (2021) 310–316.
[17] M.T. Weller, O.J. Weber, J.M. Frost, A. Walsh, Cubic perovskite structure of black formamidinium lead iodide, α-[HC (NH2) 2] PbI3, at 298 K, J. Phys. Chem. Lett. 6 (16) (2015) 3209–3212.
[18] A.Q. Alanazi, M.H. Almalki, A. Mishra, D.J. Kubicki, Z. Wang, L. Merten, M. Graetzel, Benzylammonium-mediated formamidinium lead iodide perovskite phase stabilization for photovoltaics, Adv. Funct. Mater. 31 (30) (2021), 2101163.
[19] S. Jiang, Y. Luan, J.I. Jang, T. Baikie, X. Huang, R. Li, J. Fang, Phase transitions of formamidinium lead iodide perovskite under pressure, J. Am. Chem. Soc. 140 (42) (2018) 13952–13957.
[20] M. Degani, Q. An, M. Albaladejo-Siguan, Y.J. Hofstetter, C. Cho, F. Paulus, Y. Vaynzof, 23.7% Efficient inverted perovskite solar cells by dual interfacial modification, Sci. Adv. 7 (49) (2021) eabj7930.
[21] A. Bouich, J.C. Torres, H. Chfii, J. Marí-Guaita, Y.H. Khattak, F. Baig, P. Palacios, Delafossite as hole transport layer a new pathway for efficient perovskite-based solar sells: Insight from experimental, DFT and numerical analysis, Sol. Energy 250 (2023) 18–32.
[22] Y. Xiang, X. Mo, X. Li, K. Huang, P. He, G. Dai, J. Yang, Progress on growth of metal halide perovskites by vapor-phase synthesis and their applications, J. Phys. D Appl. Phys. 55 (7) (2021), 073001.
[23] A.M. Askar, A. Karmakar, G.M. Bernard, M. Ha, V.V. Terskikh, B.D. Wiltshire, V.K. Michaelis, Composition-tunable formamidinium lead mixed halide perovskites via solvent-free mechanochemical synthesis: decoding the Pb environments using solid-state NMR spectroscopy, J. Phys. Chem. Lett. 9 (10) (2018) 2671–2677.
[24] Y. Vaynzof, The future of perovskite photovoltaics—thermal evaporation or solution processing? Adv. Energy Mater. 10 (48) (2020), 2003073.

[25] A.D. Taylor, Q. Sun, K.P. Goetz, Q. An, T. Schramm, Y. Hofstetter, Y. Vaynzof, A general approach to high-efficiency perovskite solar cells by any antisolvent, Nat. Commun. 12 (1) (2021) 1878.
[26] N. Srisamran, J. Sudchanham, C. Sriprachuabwong, K. Srisawad, P. Pakawatpanurut, K. Lohawet, A. Tuantranont, Enhanced performance and stability of fully printed perovskite solar cells and modules by ternary additives under high humidity, Energy Fuels (2023).
[27] A. Bouich, J. Marí-Guaita, B.M. Soucase, P. Palacios, Manufacture of high-efficiency and stable lead-free solar cells through antisolvent quenching engineering, Nanomaterials 12 (17) (2022) 2901.
[28] X. Guo, K. Ngai, M. Qin, X. Lu, J. Xu, M. Long, The compatibility of methylammonium and formamidinium in mixed cation perovskite: The optoelectronic and stability properties, Nanotechnology 32 (7) (2020), 075406.
[29] S. Lou, T. Xuan, J. Wang, Stability: A desiderated problem for the lead halide perovskites, Opt. Mater.: X 1 (2019), 100023.
[30] W. Rehman, R.L. Milot, G.E. Eperon, C. Wehrenfennig, J.L. Boland, H.J. Snaith, L.M. Herz, Charge-carrier dynamics and mobilities in formamidinium lead mixed-halide perovskites, Adv. Mater. 27 (48) (2015) 7938–7944.
[31] Asuo, I.M. (2021). Ambient-Processed Halide Perovskites for Photovoltaic and Optoelectronic Devices (Doctoral dissertation, Doctorat en sciences de l'énergie et des matériaux).
[32] Hu, Z. (2020). Investigations towards more performing and more stable solution-processed hybrid perovskite solar cells (Doctoral dissertation, Sorbonne université).
[33] I.H. Braddock, M. Al Sid Cheikh, J. Ghosh, R.E. Mulholland, J.G. O'Neill, V. Stolojan, P.J. Sellin, Formamidinium lead halide perovskite nanocomposite scintillators, Nanomaterials 12 (13) (2022) 2141.
[34] A. Touré, A. Bouich, B.M. Soucasse, D. Soro, Investigation of the optoelectronics properties and stability of Formamidinium lead mixed halides perovskite, Opt. Mater. 135 (2023), 113334.
[35] J.T.W. Wang, Z. Wang, S. Pathak, W. Zhang, D.W. deQuilettes, F. Wisnivesky-Rocca-Rivarola, H.J. Snaith, Efficient perovskite solar cells by metal ion doping, Energy Environ. Sci. 9 (9) (2016) 2892–2901.
[36] M. Ng, J.E. Halpert, Single crystals of mixed Br/Cl and Sn-doped formamidinium lead halide perovskites via inverse temperature crystallization, RSC Adv. 10 (7) (2020) 3832–3836.
[37] A. Bouich, J. Marí-Guaita, B. Sahraoui, P. Palacios, B. Marí, Tetrabutylammonium (TBA)-doped methylammonium lEAD iodide: high quality and stable perovskite thin films, Front. Energy Res. 10 (2022), 840817.
[38] J. Marí-Guaita, A. Bouich, B. Marí, Stability improvement of methylammonium lead iodide perovskite thin films by bismuth doping, JOM 74 (8) (2022) 3103–3110.
[39] S. Kundu, D. Zhang, A.M. Askar, E.G. Moloney, M.M. Adachi, A. Nadeem, M.I. Saidaminov, Bismuth stabilizes the α-phase of formamidinium lead iodide perovskite single crystals, ACS Mater. Lett. 4 (4) (2022) 707–712.
[40] J.L. Li, J. Yang, T. Wu, S.H. Wei, Formation of DY center as n-type limiting defects in octahedral semiconductors: the case of Bi-doped hybrid halide perovskites, J. Mater. Chem. C 7 (14) (2019) 4230–4234.
[41] E. Mosconi, B. Merabet, D. Meggiolaro, A. Zaoui, F. De Angelis, First-principles modeling of bismuth doping in the MAPbI3 perovskite, J. Phys. Chem. C. 122 (25) (2018) 14107–14112.
[42] C. Chen, J. Cheng, S. Yu, L. Che, Z. Meng, Hydrothermal synthesis of perovskite bismuth ferrite crystallites, J. Cryst. Growth 291 (1) (2006) 135–139.
[43] E. Mosconi, B. Merabet, D. Meggiolaro, A. Zaoui, F. De Angelis, First-principles modeling of bismuth doping in the MAPbI3 perovskite, J. Phys. Chem. C. 122 (25) (2018) 14107–14112.
[44] Y. Yamada, M. Hoyano, R. Akashi, K. Oto, Y. Kanemitsu, Impact of chemical doping on optical responses in bismuth-doped CH3NH3PbBr3 single crystals: carrier lifetime and photon recycling, J. Phys. Chem. Lett. 8 (23) (2017) 5798–5803.
[45] A.M. Ulatowski, A.D. Wright, B. Wenger, L.R. Buizza, S.G. Motti, H.J. Eggimann, L.M. Herz, Charge-carrier trapping dynamics in bismuth-doped thin films of MAPbBr3 perovskite, J. Phys. Chem. Lett. 11 (9) (2020) 3681–3688.
[46] R. Meng, G. Wu, J. Zhou, H. Zhou, H. Fang, M.A. Loi, Y. Zhang, Understanding the impact of bismuth heterovalent doping on the structural and photophysical properties of CH3NH3PbBr3 halide perovskite crystals with near-IR photoluminescence, Chem. Eur. J. 25 (21) (2019) 5480–5488.
[47] Y. Hu, T. Qiu, F. Bai, X. Miao, S. Zhang, Enhancing moisture-tolerance and photovoltaic performances of FAPbI 3 by bismuth incorporation, J. Mater. Chem. A 5 (48) (2017) 25258–25265.
[48] Y. Hu, T. Qiu, F. Bai, X. Miao, S. Zhang, Enhancing moisture-tolerance and photovoltaic performances of FAPbI 3 by bismuth incorporation, J. Mater. Chem. A 5 (48) (2017) 25258–25265.
[49] J.L. Li, J. Yang, T. Wu, S.H. Wei, Formation of DY center as n-type limiting defects in octahedral semiconductors: the case of Bi-doped hybrid halide perovskites, J. Mater. Chem. C. 7 (14) (2019) 4230–4234.
[50] X. Zhang, J.X. Shen, M.E. Turiansky, C.G. Van de Walle, Hidden role of Bi incorporation in nonradiative recombination in methylammonium lead iodide, J. Mater. Chem. A 8 (26) (2020) 12964–12967.
[51] S. Kundu, D. Zhang, A.M. Askar, E.G. Moloney, M.M. Adachi, A. Nadeem, M.I. Saidaminov, Bismuth stabilizes the α-phase of formamidinium lead iodide perovskite single crystals, ACS Mater. Lett. 4 (4) (2022) 707–712.
[52] N. El Messaoudi, A. El Mouden, Y. Fernine, M. El Khomri, A. Bouich, N. Faska, A. Lacherai, Green synthesis of Ag2O nanoparticles using Punica granatum leaf extract for sulfamethoxazole antibiotic adsorption: characterization, experimental study, modeling, and DFT calculation, Environmental Science and Pollution Research (2022) 1–18.
[53] S. Bouazizi, W. Tlili, A. Bouich, B.M. Soucase, A. Omri, Design and efficiency enhancement of FTO/PC60BM/CsSn0. 5Ge0. 5I3/Spiro-OMeTAD/Au perovskite solar cell utilizing SCAPS-1D Simulator, Materials Research Express 9 (9) (2022), 096402.
[54] O.A. Lozhkina, A.A. Murashkina, V.V. Shilovskikh, Y.V. Kapitonov, V.K. Ryabchuk, A.V. Emeline, T. Miyasaka, Invalidity of band-gap engineering concept for Bi3+ heterovalent doping in CsPbBr3 halide perovskite, J. Phys. Chem. Lett. 9 (18) (2018) 5408–5411.
[55] S. Kundu, D. Zhang, A.M. Askar, E.G. Moloney, M.M. Adachi, A. Nadeem, M.I. Saidaminov, Bismuth stabilizes the α-phase of formamidinium lead iodide perovskite single crystals, ACS Mater. Lett. 4 (4) (2022) 707–712.
[56] A. Bouich, J. Marí-Guaita, B.M. Soucase, P. Palacios, Bright future by enhancing the stability of methylammonium lead triiodide perovskites thin films through Rb, Cs and Li as dopants, Materials Research Bulletin 163 (2023) 112213.
[57] A. Bouich, J.C. Torres, Y.H. Khattak, F. Baig, J. Marí-Guaita, B.M. Soucase, P. Palacios, Bright Future by Controlling α/δ Phase Junction of Formamidinium Lead Iodide Doped by Imidazolium for Solar Cells: Insight from Experimental, DFT Calculations and SCAPS Simulation, Surfaces and Interfaces (2023) 103159.
[58] S. Bouazizi, A. Bouich, W. Tlili, M. Amlouk, A. Omri, B.M. Soucase, Methylammonium lead triiodide perovskite-based solar cells efficiency: Insight from experimental and simulation, Journal of Molecular Graphics and Modelling 122 (2023) 108458.